

Effect of preheating process on crystallization and optical properties of sol-gel derived ZnO semiconductor thin films

Chien-Yie Tsay · Kai-Shiung Fan · Chin-Yi Chen ·
Jyh-Ming Wu · Chien-Ming Lei

Received: 10 December 2009 / Accepted: 6 October 2010 / Published online: 23 October 2010
© Springer Science+Business Media, LLC 2010

Abstract Highly transparent ZnO semiconductor thin films were deposited onto alkali-free glass substrates by a sol-gel spin coating process. This research investigated the effects of different preheating rates (4 or 10°C/min) on the various surface morphologies, crystallization characteristics, and optical properties of these thin films. The ZnO sol was synthesized by dissolving the zinc acetate dihydrate in isopropanol (IPA), and then adding monoethanolamine (MEA). These as-coated films were preheated at 300°C for 10 min and annealed in an air ambiance at 500°C for 1 h. Experimental results revealed that the as-prepared films had a hexagonal wurtzite structure, and that the heating rates of the preheating process obviously affected the surface morphologies, crystallization qualities, and transparency levels of the thin films. A ZnO thin film preheated at 10°C/min exhibited preferential orientation along the (002) plane, a flat surface, and also achieved a high transmittance value, 92.5%, for light with a wavelength of 550 nm.

Keywords Transparent oxide semiconductor · ZnO thin films · Sol-gel method · Morphology · Optical properties

C.-Y. Tsay (✉) · K.-S. Fan · C.-Y. Chen · J.-M. Wu
Department of Materials Science and Engineering,
Feng Chia University,
No. 100, Wenhwa Rd. Seatwen,
Taichung 407 Taiwan, Republic of China
e-mail: cytsay@fcu.edu.tw

C.-M. Lei
Department of Chemical and Materials Engineering
and Master Program of Nanomaterials,
Chinese Culture University,
No. 55, Hwa-Kang Road, Yang-Ming-Shan,
Taipei 111 Taiwan, Republic of China

1 Introduction

Field effect transistors (FETs) with ZnO-based transparent channel layers are suitable for transparent electronic applications [1], such as transparent thin-film transistors (TTFTs) [2–5] and transparent electronic circuits [6, 7]. ZnO is an n-type direct band-gap semiconductor. ZnO possesses several good characteristics, including a wide energy band-gap (3.3 eV), a large free exciton binding energy (60 mV), a wide resistivity range (10^{-4} – 10^{12} Ω cm), a high electron Hall mobility ($200\text{ cm}^2/\text{V s}$), and high transparency at room temperature [8]. Due to its chemical and thermal stability, ZnO has higher carrier mobility, and lower photosensitivity than hydrogenated amorphous silicon (a-Si:H). This is noteworthy because a-Si:H thin films serve as the active channel layers in typical TFT arrays that drive liquid crystal displays (LCDs). The a-Si:H thin films used for commercial applications are almost always prepared by plasma-enhanced chemical vapor deposition (PECVD), but ZnO films offer more flexible and expandable applications because they can be fabricated with various convenient deposition processes.

Oxide semiconductor films are often made by vacuum deposition, but solution-based deposition offers a simple, low-cost alternative for large-area thin-film coatings [9]. Solution-based fabrication processes for oxide semiconductors may improve manufacturing throughputs because they enable direct pattern techniques, such as inkjet printing [10, 11]. The sol-gel method can fabricate large-area thin films with low costs and with easy control over film compositions and film thickness uniformity levels.

Ong et al. have indicated that sol-gel derived ZnO thin films with preferred orientation along the (002) plane could be important for efficient charge transport and could profoundly influence the mobility of field effect transistors

[12, 13]. The preferred crystal orientations of sol-gel derived ZnO thin films depend on sol concentrations [14–16], heat treatment conditions (preheating and annealing temperatures) [16–19], substrates used [20–22], and film thicknesses [19, 23].

When ZnO sol comes into contact with a substrate, numerous heterogeneous nucleation sites form. The crystallization of sol-gel derived ZnO thin films is determined by the nucleation step and nuclei sizes are strongly affected by the preheating process conditions [24]. Several studies have reported the influence of preheating temperatures on the properties of sol-gel derived ZnO thin films [16, 19, 25]. However, those studies did not discuss the effects of preheating rates. In the present study, transparent ZnO semiconductor thin films were prepared by a sol-gel spin coating process; we investigated how preheating rates affected the films' surface morphologies, microstructures, and optical properties.

2 Experimental procedures

Isopropanol (IPA) is a non-toxic solvent with a low boiling point. In this work, we obtained zinc acetate dihydrate ($Zn(CH_3COO)_2 \cdot 2H_2O$) that was free of chlorine ions, then dissolved that zinc acetate in IPA. Monoethanolamine (MEA) was added to stabilize this mixture; after this complex solution was stirred for 2 h at 60°C it yielded a clear and homogenous ZnO sol. The concentration of zinc ions in this ZnO sol was controlled at 0.75 M. The as-prepared ZnO sol was aged for 48 h at room temperature and then served as the coating precursor. All ZnO thin films were spin-coated onto alkali-free glass substrates (Nippon Electric Glass OA-10, with dimension 50 mm × 50 mm) at a speed of 3000 rpm for 20 s. Each as-coated film was heated from room temperature to 300°C (at a heating rate of 4 or 10°C/min), and then maintained at 300°C for 10 min. After that, the heat was increased from 300°C to 500°C (at a heating rate of 4°C/min), and then the films were maintained at 500°C for 1 h in a tube furnace under air ambiance.

The crystal structures and crystallization characteristics of the sol-gel derived ZnO thin films were identified by X-ray diffraction (XRD) using a MAC Science MXP3 X-ray diffractometer with $CuK\alpha$ radiation. Plane-view and cross-sectional micrographs of the ZnO thin films were taken with a field-emission scanning electron microscope (FE-SEM, Hitachi S-4800). The film's surface morphologies and surface roughness levels were examined by tapping mode scanning probe microscopy (SPM, Digital Instrument NS4/D3100CL/MultiMode). A UV-VIS spectrophotometer (Shimadzu UV-1601) was used to examine each film's optical transmission spectrum. The sheet resistance of each

transparent ZnO thin film was measured with a contact type resistive meter (Mitsubishi Chemical Co. MCP-HT450) at room temperature.

3 Results and discussion

The XRD patterns provided the basis for diffraction peak identification and crystal structure determination. Figure 1 shows the XRD patterns of ZnO thin films preheated at different rates (4 or 10°C/min). According to the relevant standard (JCPDS 36-1451), there are two distinct diffraction patterns that both correspond to ZnO crystal diffraction peaks. XRD results reveal all the films annealed at 500°C have a hexagonal wurtzite structure. The X-ray diffractograph of ZnO thin film preheated at 10°C/min show a high diffraction intensity for the (002) peak and obvious diffraction peaks in the (102), (103), and (112) high-index planes (spectrum (ii) in Fig. 1). Table 1 summarizes the crystal characteristics and other properties of sol-gel derived ZnO thin films. The 2nd column in Table 1 gives the relative intensity of $I_{(002)}/I_{(100)+(002)+(101)}$ which indicates that the 10°C/min preheating rate efficiently enhanced the (002) orientation. These results imply a sample preheated at 10°C/min possesses higher crystallization and exhibits preferential orientation along the (002) plane.

The crystallization of the ZnO thin films prepared from zinc acetate-isopropanol-MEA solution begins at about 250°C [16]. The crystallization and grain growth orientation of sol-gel derived ZnO thin films is determined by the nucleation step; the preheating process can be crucial to nucleation. Ohyama et al. [19] proposed that the vaporization of solvents, the decomposition of the zinc acetate, and the crystallization of the ZnO thin film may occur almost simultaneously, when the heating rate is high. Keddie et al.

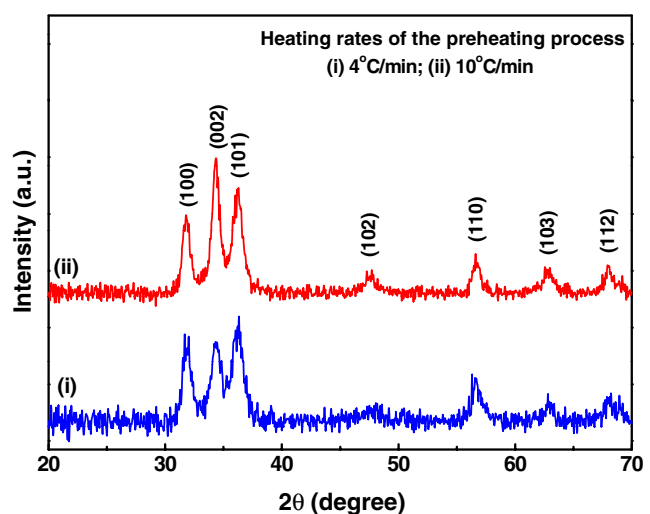


Fig. 1 XRD patterns of ZnO thin films preheated at different rates

Table 1 Crystal characteristics, RMS roughness and optical transmittance of sol-gel derived ZnO thin films

Heating rate of the preheating process (°C/min)	Relative intensity of $\frac{I_{(002)}}{I_{(100)+(002)+(101)}}$	Average crystallite size (nm)	RMS roughness (nm)	Transmittance ^a (%)
4	0.294	10.3	4.8	48.0
10	0.425	11.6	4.5	92.5

^a This table only gives transmittances for a wavelength of 550 nm

[26] also demonstrated that faster heating rate result in denser metal oxide semiconductor material. Jiwei et al. have indicated ZnO thin films possess the (002) orientation because of the highest density of Zn atoms is found along the (002) plane and thus such growth is kinetically preferred [22]. ZnO thin films with high-degree crystal orientations possess high grain-packing densities [25]; this can assist charge transport and can increase carrier mobility in the active channel layers of TFTs [12, 13].

The crystallite size (d) of each ZnO thin film was estimated using Scherrer's formula:

$$d = \frac{0.9\lambda}{B \cos \theta_B} \quad (1)$$

where λ is the X-ray wavelength of 1.5406 Å, θ_B is the Bragg diffraction angle, and B is the full width at half maximum (FWHM) of θ_B . Table 1 lists the estimated average crystallite sizes for four main diffraction peaks, (100), (002), (101) and (110), of films. The 4°C/min and 10°C/min preheating processes produced 10.3 and 11.6 nm crystallite, respectively; the faster preheating produced higher crystallization and larger average crystallite size.

Figure 2 shows the surface micrographs of ZnO thin films preheated at different rates. The plane-view SEM image of ZnO thin film preheated at 4°C/min shows fiber-like streaks on its surface (Fig. 2(a)). However, a thin film preheated at 10°C/min did not grow such streaks, and instead developed a very flat surface (Fig. 2(b)). Sol-gel derived ZnO thin films tend to exhibit fiber-like stripes or wrinkles if those films are made with insufficient OR (hydroxy or alkoxy) groups of coating precursors [27]. Our previous studies [28, 29] reported that ZnO thin films doped with metal ions can form relatively smooth surfaces, when the starting materials provide enough OR groups. This study proves that the preheating rate can unambiguously improve the surface flatness of a ZnO thin film.

Two SPM images of the ZnO thin film prepared at different heating rates for the preheating process are shown in Fig. 3. A sample preheated at 4°C/min showed a plicate structure (Fig. 3(a)). However, a film preheated at 10°C/min (Fig. 3(b)) showed no plicate structure, but rather a flat, even surface. The sample preheated at 10°C/min in Fig. 3 (b) also shows a grain orientation in the direction perpendicular to the substrate surface. The RMS roughness

values given in Table 1 that indicate samples preheated at 10°C/min had a relatively low RMS value of 4.5 nm. It is commonly thought that the RMS roughness levels of oxide films are directly related to their average crystallite sizes. Although ZnO thin films preheated at 4°C/min exhibited a finer average crystallite size, the fiber-like streaks on their surfaces gave them a RMS roughness (4.8 nm) that was higher than that of thin films preheated at 10°C/min. Figures 2 and 3 demonstrate that the preheating rates strongly influenced the surface roughness levels.

Figure 4 shows cross-sectional SEM micrographs of polycrystalline ZnO thin films. Average film thickness is about 220 and 185 nm for films preheated at 4°C/min and

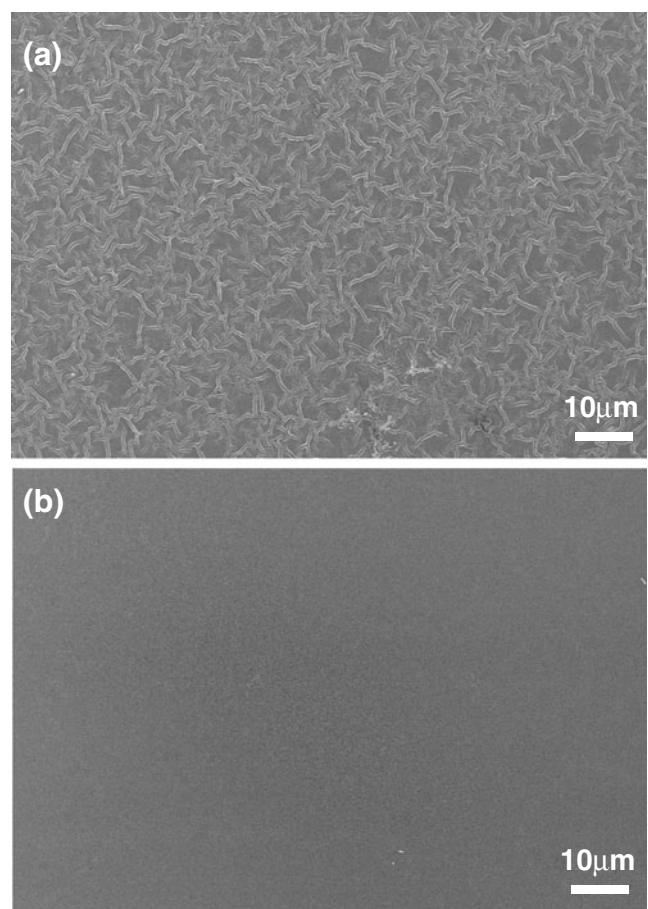


Fig. 2 Plane-view SEM micrographs of ZnO thin films, preheated at (a) 4°C/min and (b) 10°C/min

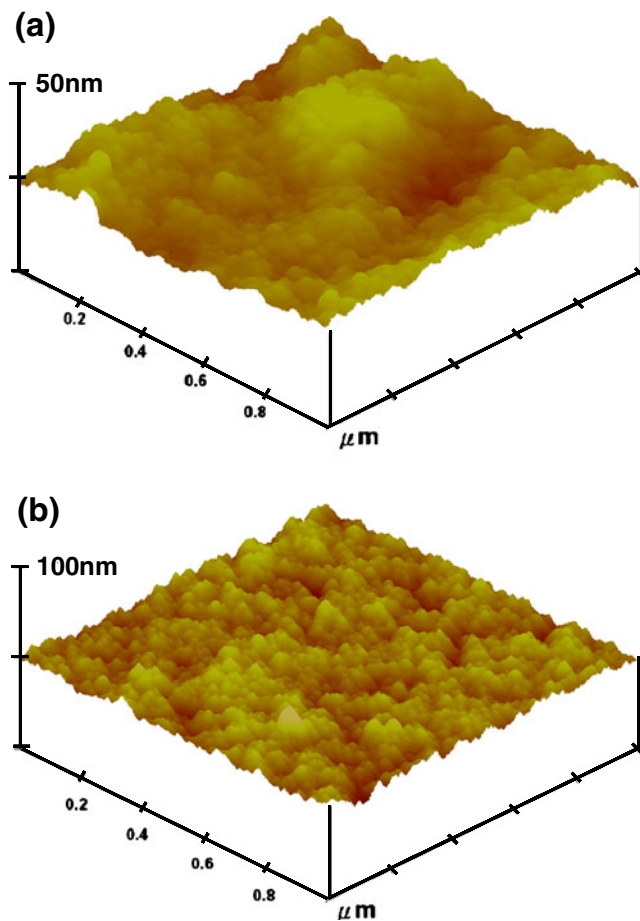


Fig. 3 SPM images of the top surfaces of ZnO thin films, preheated at (a) 4°C/min and (b) 10°C/min

10°C/min, respectively. Plane-view SEM and SPM measurements confirm that the ZnO thin film preheated at 10°C/min shows better surface flatness and more uniform film thickness than the film preheated at 4°C/min. The electrical resistivity of a ZnO thin film can be calculated by multiplying the sheet resistance by the film thickness. The resistive meter measurements indicated that a ZnO film preheated at 10°C/min has a sheet resistance of $7.6 \times 10^9 \Omega/\square$, so that film's resistivity is $1.52 \times 10^5 \Omega \text{ cm}$.

The optical transmission spectra of ZnO thin films with wavelengths from 200 to 1000 nm are shown in Fig. 5. The sample preheated at 10°C/min exhibited a sharp absorption edge at about 355 nm; the film's transmittance between 500 to 1000 nm was almost equal to the transmittance of the OA-10 glass substrates (curve (iii) in Fig. 5). Table 1 gives the transmittances for a wavelength of 550 nm; the ZnO thin film preheated at 10°C/min exhibited high transmittance of 92.5%. However, the sample preheated at 4°C/min was opaque (curve (ii) in Fig. 5). Surface flatness strongly affects the transparency levels of ZnO-based thin films [30]. Rough surfaces scatter and reflect light, thus they cause poor transparency.

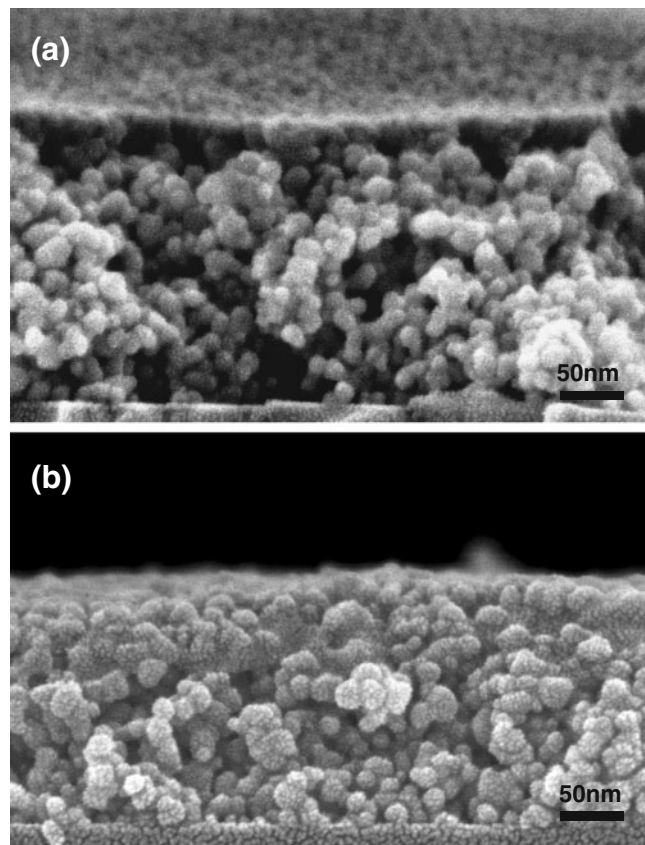


Fig. 4 Cross-sectional SEM micrographs of ZnO thin films, preheated at (a) 4°C/min and (b) 10°C/min

A direct band-gap semiconductor thin film has a transmission spectrum: the absorption edge region of that spectrum can be separated into three distinct regions [31]. The first is the weak absorption tail region, the second is

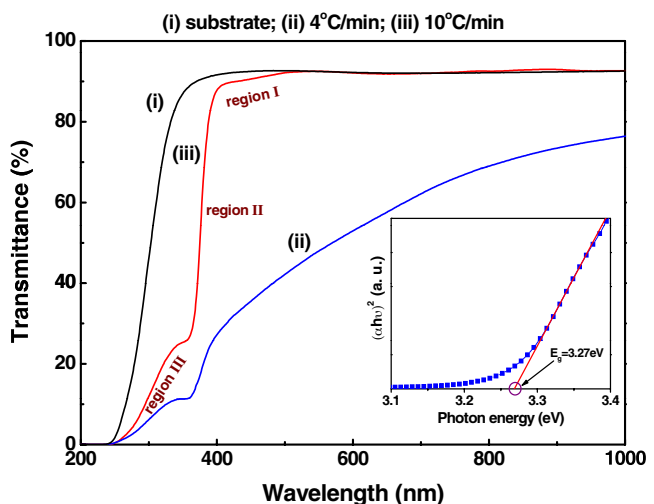


Fig. 5 Optical transmission spectra of ZnO thin films; the inset shows a plot of $(\alpha h\nu)^2$ versus photon energy for a sample preheated at a rate of 10°C/min

the exponential edge region, and the third is the high absorption region (curve (iii) in Fig. 5). In this study, the optical transmittance spectra in the near-UV region do not display high absorption characteristics (region III of curve (iii) in Fig. 5) that may be attributed to deep-level defects or to nanocrystals embedded in the ZnO thin films [32].

A semiconductor thin film has a direct-transition band-gap which can be estimated by the Tauc model [31],

$$(\alpha h\nu) = A(h\nu - E_g)^{1/2}, \quad (2)$$

where α is the absorption coefficient, $h\nu$ is the photon energy, A is a constant and E_g is the optical band-gap. The absorption coefficient (α) in the UV region of the ZO thin films can be calculated from $I = I_o e^{-\alpha t}$, where I is intensity of the transmitted light, I_o is the intensity of incident light, and t is the thickness of the thin film. The band-gap of a ZnO thin film preheated at 10°C/min was determined by extrapolation of the straight section of the plot of $(\alpha h\nu)^2$ versus photo energy (insert of Fig. 5). The E_g value of 3.27 eV was determined to be the same as in previous reports [33, 34].

The background electronic concentrations of ZnO semiconductor thin films must be reduced in order to reduce the off-state drain current and to increase ZnO-TFTs carrier mobility [35]. The present study has developed a transparent oxide semiconductor (TOS) thin film that might be applied in the active channel layers of transparent thin film transistors (TTFTs).

4 Conclusions

Transparent semiconductor ZnO thin films have been successfully prepared with a sol-gel method and a spin-coating technique. The nanocrystalline ZnO thin films exhibited a hexagonal wurtzite structure. We demonstrated the preheating process was an important factor in the formation of these high-quality ZnO thin films. The alteration of preheating rate from 4 to 10°C/min evidently enhanced the crystallization, improved surface flatness, and produced high transparency in the visible range. In the present study, the ZnO thin film sample preheated at 10°C/min exhibited preferred orientation along the (002) plane, an optical transmittance of 92.5%, a RMS roughness of 4.5 nm, and a resistivity of $1.52 \times 10^5 \Omega \text{ cm}$.

Acknowledgments The authors gratefully acknowledge the financial support of the National Science Council of the Republic of China under Contract No. NSC 95-2221-E-035-006.

References

1. J.F. Wager, *Science* **300**, 1245 (2003)
2. E. Fortunato, P. Barquinha, A. Pimentel, A. Gonçalves, A. Marques, L. Pereira, R. Martins, *Adv. Mater.* **17**, 590 (2005)
3. T. Kamiya, H. Hiramatsu, K. Nomura, H. Hosono, *J. Electroceram.* **17**, 267 (2006)
4. H.C. Cheng, C.F. Chen, C.Y. Tsay, *Appl. Phys. Lett.* **90**, 012113 (2007)
5. S.H. Park, C.S. Hwang, M. Ryu, S. Yang, C. Byun, J. Shin, J.I. Lee, K. Lee, M.S. Oh, S. Im, *Adv. Mater.* **21**, 678 (2009)
6. M. Ofuji, K. Abe, H. Shimizu, N. Kaji, R. Hayashi, M. Sano, H. Kumomi, K. Nomura, T. Kamiya, H. Hosono, *IEEE Electron Device Lett.* **28**, 273 (2007)
7. R.E. Presley, D. Hong, H.Q. Chiang, C.M. Hung, R.L. Hoffman, J.F. Wager, *Solid State Electron.* **50**, 500 (2006)
8. S.J. Pearton, D.P. Norton, K. Ip, Y.W. Heo, T. Steiner, *J. Vac. Sci. Technol. B* **22**, 932 (2004)
9. S. Lee, Y. Jeong, S. Jeong, J. Lee, M. Jeon, J. Moon, *Superlattices Microstruct.* **44**, 761 (2008)
10. S.T. Meyers, J.T. Anderson, C.M. Hung, J. Thompson, J.F. Wager, D.A. Kesler, *J. Am. Chem. Soc.* **130**, 17603 (2008)
11. J.J. Schneider, R.C. Hoffmann, J. Engstler, O. Soffke, W. Jaegermann, A. Issanin, A. Klysycz, *Adv. Mater.* **20**, 3383 (2008)
12. B.S. Ong, C. Li, Y. Li, Y. Wu, R. Loutfy, *J. Am. Chem. Soc.* **129**, 2750 (2007)
13. C.S. Li, Y.N. Li, Y.L. Wu, B.S. Ong, R.O. Loutfy, *J. Phys. D: Appl. Phys.* **41**, 125102 (2008)
14. S. O'Brien, L.H.K. Koh, G.M. Crean, *Thin Solid Films* **516**, 1391 (2008)
15. M. Dutta, S. Mridha, D. Basak, *Appl. Surf. Sci.* **254**, 2743 (2008)
16. Y.S. Kim, W.P. Tai, S.J. Shu, *Thin Solid Films* **491**, 153 (2005)
17. M.W. Zhu, J. Gong, C. Sun, J.H. Xia, X. Jiang, *J. Appl. Phys.* **104**, 073113 (2008)
18. D. Bao, H. Gu, A. Kuang, *Thin Solid Films* **312**, 37 (1998)
19. M. Ohyama, H. Kozuka, T. Yoko, *Thin Solid Films* **306**, 78 (1997)
20. R. Ghosh, D. Basak, S. Fujihara, *J. Appl. Phys.* **96**, 2689 (2004)
21. S. Chakrabarti, D. Ganguli, S. Chaudhuri, *Mater. Lett.* **58**, 3952 (2004)
22. Z. Jiwei, Z. Liangying, Y. Xi, *Ceram. Inter.* **26**, 883 (2000)
23. M.H. Aslan, A.Y. Oral, E. Menşur, A. Güll, E. Başaran, *Solar Energy Mater. Solar Cells* **82**, 543 (2004)
24. Y. Ohya, H. Saiki, T. Tanaka, Y. Takahashi, *J. Am. Ceram. Soc.* **79**, 825 (1996)
25. M. Ohyama, H. Kozuka, T. Yoko, *J. Am. Ceram. Soc.* **81**, 1622 (1998)
26. J.L. Keddie, E.P. Giannelis, *J. Am. Ceram. Soc.* **74**, 2669 (1991)
27. G.W. Scherer, *J. Sol-Gel Sci. Tech.* **8**, 353 (1997)
28. C.Y. Tsay, M.C. Wang, S.C. Chiang, *J. Electron. Mater.* **38**, 1962 (2009)
29. C.Y. Tsay, H.C. Cheng, Y.T. Tung, W.H. Tuan, C.K. Lin, *Thin Solid Films* **517**, 1032 (2008)
30. J.H. Lee, K.H. Ko, B.O. Park, *J. Cryst. Growth* **247**, 119 (2003)
31. J. Tauc, R. Grigorovici, A. Vancu, *Phys. Stat. Sol.* **15**, 627 (1966)
32. S.T. Tan, B.J. Chen, X.W. Sun, W.J. Fan, H.S. Kwok, X.H. Zhang, S.J. Chua, *J. Appl. Phys.* **98**, 013505 (2005)
33. G. Srinivasan, J. Kumar, *J. Cryst. Growth* **310**, 1841 (2008)
34. R.E. Marotti, C.D. Bojorge, E. Broitman, H.R. Cánepa, J.A. Badán, E.A. Dalchiele, A.J. Gellman, *Thin Solid Films* **517**, 1077 (2008)
35. E. Fortunato, P. Barquinha, A. Pimentel, A. Gonçalves, A. Marques, L. Pereira, R. Martins, *Thin Solid Films* **487**, 205 (2005)